Light charged-particle production from neutron bombardment of silicon up to 60 MeV: Role of level densities and isospin

F. B. Bateman,* R. C. Haight, M. B. Chadwick, and S. M. Sterbenz
Los Alamos National Laboratory, Los Alamos, New Mexico 87545

S. M. Grimes
Ohio University, Athens, Ohio 45701

H. Vonach
Institut für Radiumforschung und Kernphysik, A1090 Vienna, Austria
(Received 7 May 1999; published 15 November 1999)

Inclusive light charged-particle emission spectra and cross sections from neutron bombardment of silicon were measured at 30°, 60°, 90°, and 135° over the neutron energy range from threshold to approximately 60 MeV. Source neutrons, continuous in energy, were provided by the spallation neutron source of the Los Alamos Weapons Neutron Research facility. Comparisons of our alpha-particle data with Hauser-Feshbach calculations, which include multistage emission processes and preequilibrium particle emission, indicate that the majority of alpha particles result from compound nuclear reactions. For proton and deuteron emission, direct and preequilibrium processes contribute significantly to the emission cross section. These data provide rigorous tests for the calculations while helping to guide the selection of input parameters such as nuclear level densities. The effects of assuming partial or complete isospin conservation are shown to be important for these reactions. [S0556-2813(99)02012-9]

PACS number(s): 25.40.−h

I. INTRODUCTION

An increased understanding of neutron-induced charged-particle producing reactions on silicon is important not only for basic physics but also for applications. The cross sections, angular distributions, and spectra can constrain nuclear model calculations in a region where a significant body of complementary information exists. Information on nuclear level densities and on the role of isospin conservation can therefore be derived and compared with previously obtained systematics and with theoretical models. Silicon is also of great applied interest in the semiconductor industry and in detectors for physics experiments. Neutron-induced reactions have been known for many years to be responsible for producing errors in semiconductor memories [1] and, in fact, integral testing of computer components by neutron irradiations is now common [2,3]. An understanding of the basic interactions might lead to a better design of semiconductor architectures which would be more resistant to radiation damage by neutrons [4].

Neutron-induced charged-particle producing reactions on Si have been studied previously, mostly for neutron energies below 15 MeV, but recently also at selected higher energies. At low energies, proton production on ^{28}Si can be measured by activation methods for neutron energies where only the ^{28}Si$(n,p)^{28}$Al channel is open to proton emission. This technique cannot be used for the ^{28}Si$(n,\alpha)^{25}$Mg reaction since the residual nucleus is stable. At higher bombarding energies, many charged-particle producing channels such as

$(n,n'p)$ and $(n,n'\alpha)$ lead also to stable residual nuclei. Total charged-particle production can be measured using mass spectrometry techniques, but these require monoenergetic sources which are usually not of sufficient intensity except at 14 MeV. Thus, the only practical means to measure charged particles produced by neutron bombardment over a range in projectile energy is by direct measurement of the emitted particles.

The present measurements extend from threshold to 50 MeV (and to 60 MeV for alpha particles), a much wider energy range than in previous works. They therefore provide information on the reaction mechanisms involved and their dependences on the projectile's incident energy. The present data fill large regions where there were only fragmentary data previously, such as between 15 and 50 MeV. Furthermore, measurements of all of the light charged particles can be used to test the predictive capability of model calculations in a more stringent manner.

Data on emission of light charged particles can provide information on nuclear level densities through nuclear model calculations based on Hauser-Feshbach theory [5], a formalism describing reaction processes which involve the formation and decay of a compound nucleus. Nuclear level densities enter explicitly into the Hauser-Feshbach cross section formula. Information on nuclear level densities may be obtained by studying the magnitude and shape of continuum charged-particle emission spectra within this well-defined theoretical framework. Level densities of residual nuclei populated through a specific reaction channel can be derived for excitation energies between the region of resolved levels and the neutron binding energy. Information on the level density in the target nucleus is also available from the charged-particle production cross sections, since neutron emission (the competing channel) is the dominant decay mode of the compound nucleus, and this latter process yields

60 064609-1

a residual nucleus which is the same as the target. In this case the average excitation energy reached is approximately $U = E_0 - 2T$ [6], where E_0 is the incident neutron energy and T the nuclear temperature at E_0.

Most existing level density information has been obtained from neutron resonance studies at or near the neutron binding energy. Level densities for some nuclides have been derived at higher energies from fluctuations in cross sections analyzed by Ericson theory [7,8]. Such results have been obtained for nuclei formed as compound nuclei and include ^{28}Al [9], ^{28}Si [10], and ^{29}Si [11]—nuclei particularly important in the present analysis. It is hoped that our program to measure $(n, \text{charged-particle})$ cross sections on several targets, combined with theoretical efforts, can help provide a framework for a global level density prescription.

In this paper, an experiment to measure inclusive charged-particle production by neutrons on silicon is described, and results are presented and compared with statistical and preequilibrium model calculations.

II. EXPERIMENTAL PROCEDURE

Experimental data were obtained at the Weapons Neutron Research (WNR) facility of the Los Alamos Neutron Science Center (LANSCE) [12] in an experimental arrangement that was described generally in a previous report [13]. Only a brief description will be given here, and specific features of the present measurement will be emphasized.

Source neutrons are produced by directing the 800 MeV proton beam from the LANSCE accelerator to a 7 cm long cylindrical tungsten target. The proton beam is bunched to a width of ≈ 200 ps, with a typical repetition rate of 35 000 pulses/s. Spallation reactions in the target result in the production of several neutrons per beam proton, yielding an intense neutron spectrum continuous in energy from a few hundred keV up to several hundred MeV. A beam path at an angle of 90° to the primary beam was chosen to provide the largest neutron flux below 60 MeV. A collimator system restricted the beam dimensions at the sample position to a 50×50 mm square with 10 mm cut off each corner to give a pattern appropriate to the circular targets oriented at 42° with respect to the beam. The collimated beam shape has been reported previously [14].

The neutron-induced reactions took place in the previously described evacuated chamber [13]. The distance from the neutron source to the silicon sample was 9.123 m. A fission chamber containing a ^{235}U fission foil, used to monitor the neutron flux, was placed beyond the chamber at a distance of 10.10 m from the source.

Two sample foils of very different thickness, consisting of natural silicon, were used in the experiment. Silicon is nearly monoisotopic, comprised 92% of ^{28}Si. For the first set of measurements, a thick foil with an areal density of 9.78 mg/cm^2 was used. This sample caused the alpha-particle detection threshold to be too high, and we subsequently obtained a much thinner sample with an areal density of 0.320 mg/cm^2. This latter sample provided all of the alpha-particle data together with data at the lowest proton energies. The

thicker sample was used to obtain most of the proton and all of the deuteron data.

The detector arrangement for these measurements consisted of four three-element telescopes located at 30°, 60°, 90°, and 135° to the incident beam direction. For the present measurements, we used two types of detector arrangements, each consisting of three elements: The first element of the telescope (ΔE) consisted of either a thin-window low-pressure gas proportional counter, to detect low-energy alpha particles, or a thin (≈ 100 μm) silicon surface barrier detector. Xenon gas at a typical pressure of 25 Torr was used in the proportional counters. Silicon surface barrier detectors, 450 mm$^2 \times 500$ μm, served as the second detector of the telescope (S). These first two detectors operated in an ΔE-E mode to measure protons up to ≈ 8 MeV and alpha particles up to ≈ 33 MeV. Beyond these energies CsI(Tl) detectors, coupled to photodiodes, were used as the third element (C). This arrangement allowed the detection of protons up to 50 MeV, with the C and S detectors operating in ΔE-E mode. For particles that stopped in the S detectors, a clear identification of all $Z=1$ and $Z=2$ particles was achieved when silicon detectors were used as the first element of each telescope. To detect low-energy particles such as protons below 4 MeV, proportional counters were used. These counters gave good separation between $Z=1$ and $Z=2$ particles but not between protons and deuterons. Because deuteron production cross sections are much smaller than those for protons, we assume that all the $Z=1$ particles below 4 MeV are protons. Production of ^{3}H and ^{3}He was observed in the silicon ΔE-detector data to be much smaller than for the other hydrogen and helium isotopes, and the present data on mass-3 isotopes is not otherwise useful here because of very large statistical uncertainties.

A continuous energy spectrum offers a distinct advantage over a monoenergetic source since it allows emission cross sections to be measured over all neutron energies simultaneously. Neutron energies were determined by time of flight over the 9.123 m flight path. With a beam micropulse spacing of 1.8 μs, the frame overlap caused by neutrons from a previous beam burst occurs below 200 keV, much lower than the thresholds for $(n, \text{charged-particle})$ reactions on ^{28}Si. All timing signals were derived from the S detectors, and the time calibrations were performed using a commercial time calibrator. The overall time resolution of the system, inferred from the width of the prompt gamma-ray peak, was determined to be ~ 3 ns. This gives rise to a neutron energy resolution of 100, 810, and 3210 keV at neutron energies of 5, 20, and 50 MeV, respectively.

Energy calibration of the S detectors was accomplished using a mixed ^{228,229}Th alpha-particle source. The system response was observed to be extremely linear over the range in alpha calibration energies from ~ 4.9 to ~ 8.8 MeV. While these calibrations are fairly routine for the silicon detectors, this is not the case for the CsI(Tl) detectors. In principle, the alpha source could be used to calibrate the CsI(Tl) detectors as well. Their light output, however, is known to vary for different charged-particle species [15], and hence this calibration would only be valid for alpha particles. Also, since the response is nonlinear, use of the alpha source would result in an invalid calibration at higher energies. Eventually it was decided that the best technique for calibrating the-

CsI(Tl) detectors would be to use the kinematics of the reactions on silicon and determine the end point energy of the emitted particle as a function of time of flight. To obtain the proper calibration energies, ejectile energies derived from reaction kinematics had to be corrected for energy loss in the target (assuming the particles were produced halfway in the target), the ΔE detector, and the S detector. Separate calibrations for protons, deuterons, and alpha particles were obtained using this method.

Standard NIM electronics were used to acquire the data, and a detailed description will be given elsewhere. After amplification and shaping, the analog pulse-height signals were digitized using FERA[1] analog-to-digital converters. Timing logic signals were processed with a FERA time digitizer module. Events were buffered to a FERA memory module and read out through a CAMAC data bus after every beam macropulse.

Data acquisition, readout, and sorting were handled by the XSYS data acquisition system [16] operating in event mode. An XSYS event handling routine was responsible for preprocessing and sorting the data, allowing on-line viewing of the spectra and for writing the event data to disk. These disk files were later used to replay the data.

In replaying the event-mode data, events were sorted according to gates placed around the particle of interest in the two-dimensional pulse height arrays, ΔE vs S and S vs C. To replay the low-energy proton and deuteron data, it was necessary to eliminate charged-particle events where the particles did not stop in the S detector and hence did not deposit their full energy. This was accomplished by requiring that no corresponding event was present in the C detector, implying that the particle stopped in the S detector. This difficulty also existed for higher-energy protons and deuterons which ''punched'' through the C detector. A neutron energy upper limit of ~ 60 MeV was applied to ensure that all particles stopped in the C detector. Particle energies were corrected for energy loss in the detectors and target (assuming all particles were produced halfway through the target). In order to associate the time of flight of an event with an incident neutron energy, a correction was made for the ejectile flight time from sample to detector, determined by the particle energy.

The data were binned in neutron energy bins with widths of 0.5–2 MeV. The widths were chosen to provide good statistical accuracy while not masking any short-range structure which might be present in the cross section. The final cross section results appear to vary smoothly with neutron energy and we are confident that this binning faithfully represents the data.

III. STATISTICAL MODEL CALCULATIONS

A. General

Model calculations for neutron reactions on silicon were performed with the GNASH code [17], which applies Hauser-

---

Feshbach compound nucleus theory to describe the decay of equilibrated nuclei and the exciton model to describe the emission of higher-energy preequilibrium ejectiles in the early stage of the reaction. The Hauser-Feshbach calculation accounts for sequential multiparticle and gamma-ray decay until secondary emission is complete and a residual nucleus is left in its ground state. The emission of preequilibrium cluster particles (alpha particles, deuterons, etc.) was calculated with the model of Kalbach [18], which is based primarily on phase space considerations and includes a pickup model for deuteron emission. Furthermore, multiparticle nucleon preequilibrium emission, which becomes important above 40–50 MeV incident energy, is included using the model of Ref. [19].

The Hauser-Feshbach calculations depend sensitively on the input ingredients, i.e., level densities and transmission coefficients from the optical model, which are described in detail below. Usually, these calculations do not include considerations of isospin conservation. As this effect may be significant for neutron reactions on silicon, the impact of isospin conservation effects is discussed in more detail later in this paper.

B. Level densities

The Hauser-Feshbach calculations made use of nuclear level densities from the Gilbert-Cameron [20] approach— that is, a Fermi-gas form at high excitation energies matched on to a constant-temperature form at lower energies. The matching energy was chosen automatically for each compound nucleus so that the level density and its first derivative were continuous and, at the lowest excitation energies, the constant-temperature value matched the experimental level density from the known low-lying nuclear levels.

We made use of experimental information on the total level density where available, choosing the level density parameter and the pairing energy such that the results from the Fermi-gas analytic expression approximated the experimental level density data. These data are described below. Making use of such level density data is particularly important for an accurate calculation of alpha-particle and proton emission, since these cross sections are small compared to the neutron-emission competition channel, and depend sensitively on the level densities describing the accessible phase space.

For the ^{28}Si nucleus (produced after single neutron emission), Ref. [10] presented experimental total level density results in the excitation energy region 20–26 MeV from Ericson fluctuation analyses and below 12 MeV from level counting. For ^{28}Al (produced after single-proton emission), there are total level densities from Ericson fluctuation measurements by Abfalterer et al. [9] for the excitation energy region 13–21 MeV and from level counting below 10 MeV. The level densities used in our calculations, where the level density parameters were chosen to fit these data, are shown in Fig. 1.

For ^{25}Mg (produced after single-alpha emission), data exist for the nuclear level density at the neutron separation energy from the measured spacing of s-wave neutron reso-
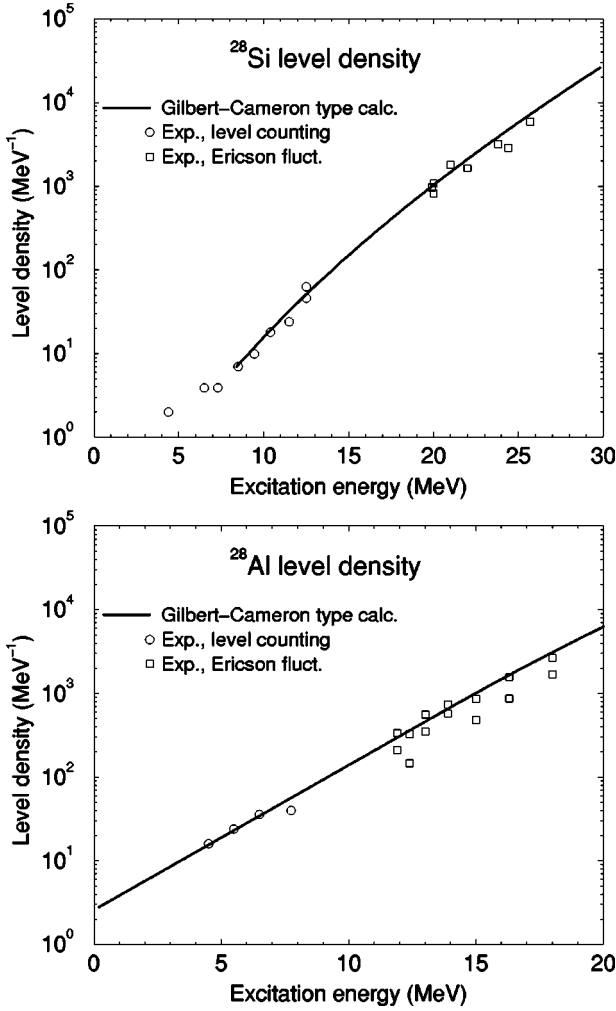
FIG. 1. Calculated level densities compared with measurements for ^{28}Si and ^{28}Al. Level density parameters $a = 3.35$ MeV^{-1}, $\Delta = 3.89$ MeV (for ^{28}Si) and $a = 3.55$ MeV^{-1}, $\Delta = 0$ MeV (for ^{28}Al) were used in the Fermi-gas expression. The calculations do not use the statistical level density model at low energies in the discrete level region where known levels were used directly in the Hauser-Feshbach analyses.

nances. However, the statistically small number of resonances (4) owing to the light mass of ^{25}Mg results in a wide range of values from different analyses (e.g., $D_0 = 470 \pm 140$ keV from an Obninsk Nuclear Data Group compilation compared to $D_0 = 234$ keV from a Chinese Nuclear Data Group compilation; see Ref. [21]). Furthermore, use of s-wave resonance spacing information to infer total level densities for light nuclei is complicated by the fact that the positive-negative parity ratio may not be 0.5:0.5. We therefore used level density parameters ($a = 4.325, \Delta = 1.75$) for ^{25}Mg that resulted in agreement with alpha production measurements for neutron energies below 10 MeV, where only the (n,α) reaction contributes, giving $D_0 = 374$ keV, which is consistent with the above-measured values.

Using the above experimental level density information significantly constrained the Hauser-Feshbach calculations for incident energies where multiparticle emission cannot occur (below about 10 MeV). At higher incident energies, mul-

tiparticle emission results in the excitation of compound nuclei for which in many cases no experimental level density data exist. Level density parameters for these nuclei were obtained from systematics [22], and are therefore expected to be less precise.

For each decaying compound nucleus, low-lying nuclear levels, along with their spins, parities, and decay branching ratios, were used in the Hauser-Feshbach calculations and in the gamma-ray decay cascades. This information was taken from the Evaluated Nuclear Structure Data File (ENSDF) compilation [21] for excitation energies where the information was judged to be ''complete'' (where all spins and parities are known, and where the density of these levels is still rising exponentially).

Finally, to assess the sensitivity of the calculated results to the level density parameters used, we have also performed a set of calculations that make use of the level density parameters by Huang, Grimes, and Massey (set A) [23], specifically developed for the $A = 20$–40 region. The systematics for these parameters were based on the analysis of Braga-Marcazzan and Milazzo-Colli [24] who analyzed Ericson fluctuation data from a number of papers to obtain individual level density ''a'' values for a number of nuclei in the mass region $20 \leq A \leq 50$. These were deduced with the assumption that the energy shift was that due to pairing energy only and that the pairing energy shift was that given by Gilbert and Cameron [20]. The function $\alpha A + B$ was fit by Huang, Grimes, and Massey [23] to these a values and the results compared with densities at low energies deduced from level counting. This comparison showed that the slopes were reasonable, but that there was an additional energy shift required. A systematical procedure for calculating these shifts was developed. In the region $20 \leq A \leq 40$ a formula has been found to represent a, and a technique comparing the actual mass of the ground state to systematics gives the energy shift, which includes pairing and shell contributions. The a parameter is given by [23]

$$a = 0.086A + 1.18, \tag{1}$$

and the energy shift, by $\Delta = M_{\text{expt}} - M_{\text{syst}}$, where M_{expt} is the experimental ground-state binding energy, and M_{syst} is obtained from a liquid-drop expression

$$M_{\text{syst}} = 15.598A - 17.97A^{2/3} - (0.8176 - 0.6457A^{-1/3})\frac{Z^2}{A}$$
$$- 24.1\frac{(N-Z)^2}{A}, \tag{2}$$

in units of MeV.

C. Optical model calculations

Coupled channel optical model calculations were performed with the ECIS code [25] to determine transmission coefficients and inelastic neutron scattering cross sections to low-lying collective levels (a rotational 0^+, 2^+, 4^+ band and a vibrational 3^- state). Our starting point was the global medium-energy optical potential of Madland [26], based on earlier work by Schwandt for neutrons above 46 MeV and
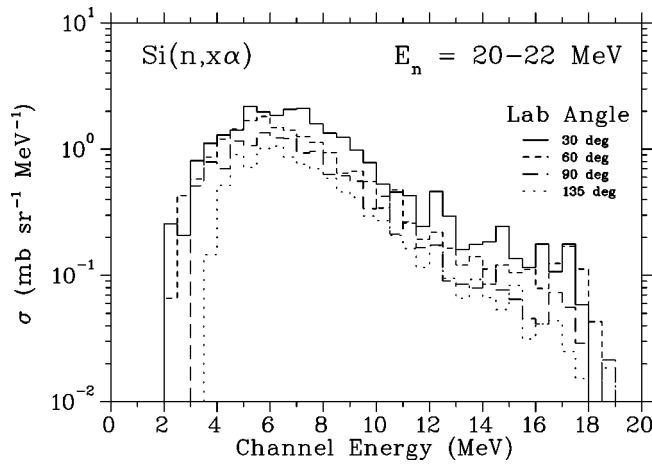
FIG. 2. Typical alpha-particle emission spectra at all four emission angles for incident neutron energies of 20–22 MeV.

FIG. 3. Typical proton-emission spectra at all four emission angles for incident neutron energies of 45–47 MeV.

the Wilmore-Hodgson potential for lower neutron energies (the reaction cross sections are continuous for these two potentials at 46 MeV). The depths of the imaginary components of these spherical potentials were then reduced by 20% to account approximately for the explicit calculation of inelastic scattering to the coupled states. Deformation parameters were chosen to reproduce the ENDF/B-VI inelastic cross sections at 20 MeV, resulting in values of $\beta_2 = -0.365$ and $\beta_4 = +0.22$, in reasonable agreement with Alarcon and Rapaport's values of -0.37 and 0.17, respectively [27]. A vibrational distorted-wave Born approximation (DWBA) calculation was performed for the 3^- state, resulting in $\beta_3 = 0.235$ (Alarcon and Rapaport obtained 0.23) [27].

For protons, the global medium-energy optical potential [26] was used above 28 MeV and the Becchetti-Greenlees [28] potential was used for lower proton energies. Again, the transition region to the medium-energy potential was chosen to give continuity in the reaction cross section. For deuterons the global potential of Perey and Perey [29] was used, and for alpha particles the global potential of McFadden and Satchler was used [30].

IV. RESULTS AND DISCUSSION

A. Experimental results

The results presented in the following section are typical, and we have attempted to provide a representative sample of the many data obtained in this work. Shown are angle- and energy-integrated cross sections as a function of incident neutron energy, selected emission spectra, and selected angular distributions for proton, deuteron, and alpha-particle production. Comparisons with literature values and theoretical calculations (see Secs. IV B and IV C) are made whenever possible. The entire data set is available from the National Nuclear Data Center at Brookhaven National Laboratory.

Typical emission spectra are given in Figs. 2, 3, and 4 for alpha particles, protons, and deuterons, respectively. The data are expressed in terms of channel energy, assuming two-body kinematics, to facilitate comparisons with calculational
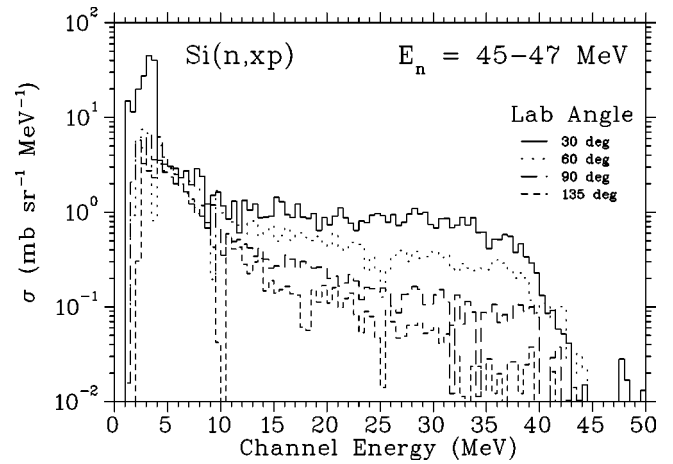
models and some literature values. The present results were obtained by combining data from the thin and thick targets. The thick-target data were taken with a silicon ΔE detector which had a threshold for detecting protons of about 4 MeV. Below this energy we use data from the thin target, where the ΔE detectors were the proportional counters with a threshold energy of about 1.5 MeV. Despite this low threshold for detecting protons, there is the possibility that protons of even lower energy were missed because of the low Coulomb barrier and the reaction kinematics. We discuss this effect below.

Figure 5 compares proton-emission spectra at 14.1 MeV with those obtained by Colli *et al.* [31] at three laboratory emission angles. There is reasonable agreement between the two data sets. Our data from the proportional counters are given separately from those with silicon ΔE detectors, and the two sets show smooth matching at 4 MeV. Angle-integrated spectra for proton and alpha emission were obtained by fitting the double-differential data with Legendre polynomials up to second order at each channel energy. A sample fit for protons is given in Fig. 6. The angle-integrated cross section is obtained by integrating over all angles. The
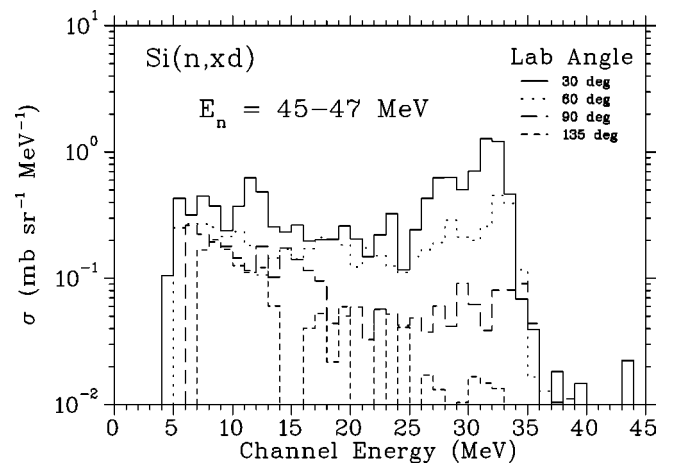

FIG. 4. Typical deuteron-emission spectra at all four emission angles for incident neutron energies of 45–47 MeV.
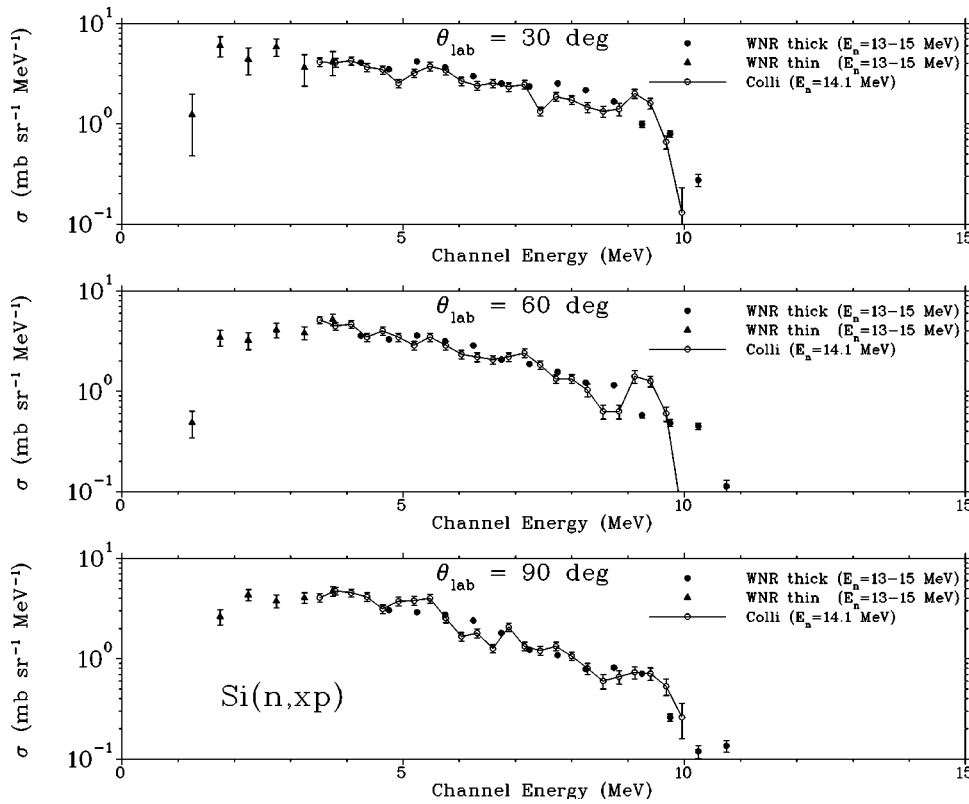
FIG. 5. Double-differential cross sections for $E_n = 13$–15 MeV obtained at laboratory angles of 30°, 60°, and 90° compared to the 14.1 MeV results of Colli *et al.* [31].

error in the cross section is given by the error returned by the least-squares fitting routine.

Angle-integrated cross sections for alpha-particle emission are shown in Fig. 7 for various neutron energies. All spectra exhibit a prominent evaporation peak at ~6 MeV, independent of bombarding energy, characteristic of a compound nuclear emission process. The maximum alpha-particle energy increases correspondingly with incident neutron energy. For $E_n \sim 15$ MeV and above, the results show a significant high-energy tail characteristic of preequilibrium processes. Comparable angle-integrated spectra for proton emission are given in Fig. 8. The fact that these spectra extend beyond the calculated end points reflects the energy

resolution of the CsI(Tl) detectors and the finite neutron energy bin width. These spectra exhibit similar characteristics to the alpha-particle results, containing a compound emission peak and a higher-energy preequilibrium component as the bombarding energy increases. This higher-energy tail is more prevalent for proton emission, because it is more probable for a proton, compared to an alpha cluster, to be emitted in the early preequilibrium phase of the reaction.

The deuteron-emission spectra exhibit a rather sharp angular dependence, incompatible with the Legendre fitting method. Thus the deuteron angle-integrated spectra were obtained with a simple numeric integration over the four angles θ weighted by $\sin(\theta)$. Results of angle-integrated cross sections for deuterons are given in Fig. 9 for several incident neutron energies. The most striking feature of these spectra, distinguishing them from proton and alpha emission, is a prominent peak observed at higher ejectile energies. This component of the spectrum is the result of a direct reaction process in which the incident neutron picks up a proton in the nucleus.

Angular distributions for alpha particles are presented in Fig. 10 for different regions of the emission spectrum and various neutron energies. Figure 11 depicts proton angular distributions under similar conditions. As expected, the spectra become more forward peaked as the channel energy increases, typical of a precompound emission process. It is somewhat surprising that the spectra exhibit a significant anisotropy even in the compound region of the emission spectrum. This trend has also been observed previously by other authors [32]. At higher channel energies the proton angular distributions appear to be more forward peaked, suggesting
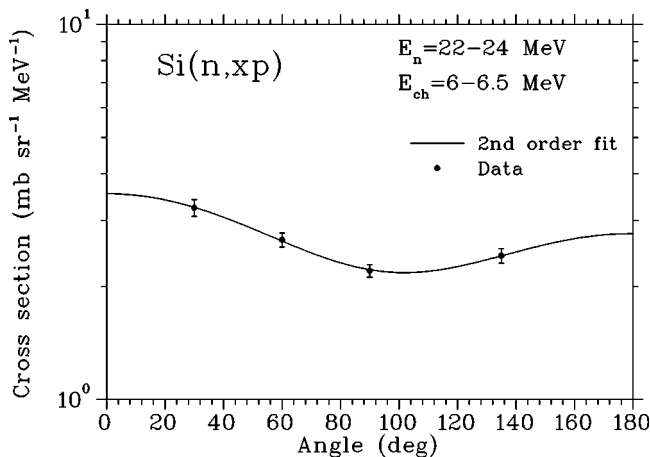

FIG. 6. Sample Legendre polynomial fit for proton emission. Legendre polynomials up to order 2 are included in the fit.
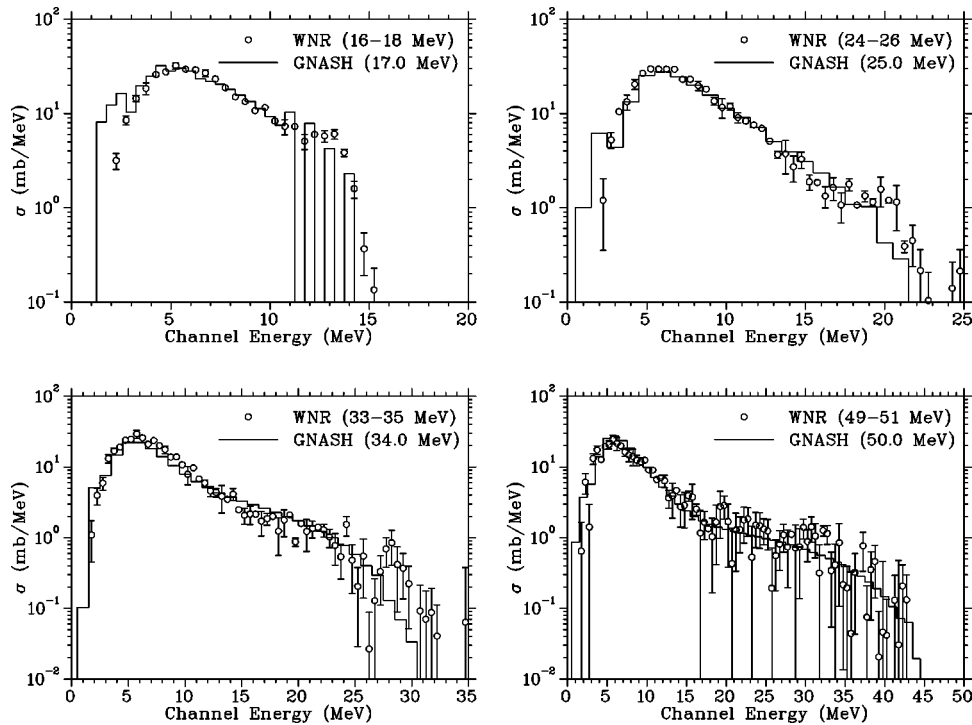
FIG. 7. Angle-integrated alpha-particle emission spectra for neutron energies of 16–18, 24–26, 33–35, and 49–51 MeV. The solid line depicts the results of GNASH calculations performed at the midpoint of the respective neutron energy bin.

that nonequilibrium processes play a larger role in proton emission. In addition, the degree of forward peaking appears to be characterized more by the emission energy of the ejectiles than by the incident neutron energy, a phenomenon commonly referred to as Kalbach systematics [33]. Proton angular distribution data obtained by Hassler and Peck [34] at 14.4 MeV are compared with results of the present experiment in Fig. 12 for proton energies above 3 MeV, the threshold for Ref. [34]. Good agreement between the two data sets is seen.

Sample angular distributions for deuteron production are shown in Fig. 13. This figure illustrates the contributions of the various reaction mechanisms to the emission cross section. In the ejectile energy region of 7–10 MeV, near the compound-emission peak, the angular distributions are fairly isotropic. As the emission energy increases, the spectra tend to become more forward peaked, as expected. For certain neutron energies, the emission energy corresponds to the region of the direct reaction peak, resulting in a further enhancement of the cross section in the forward direction.
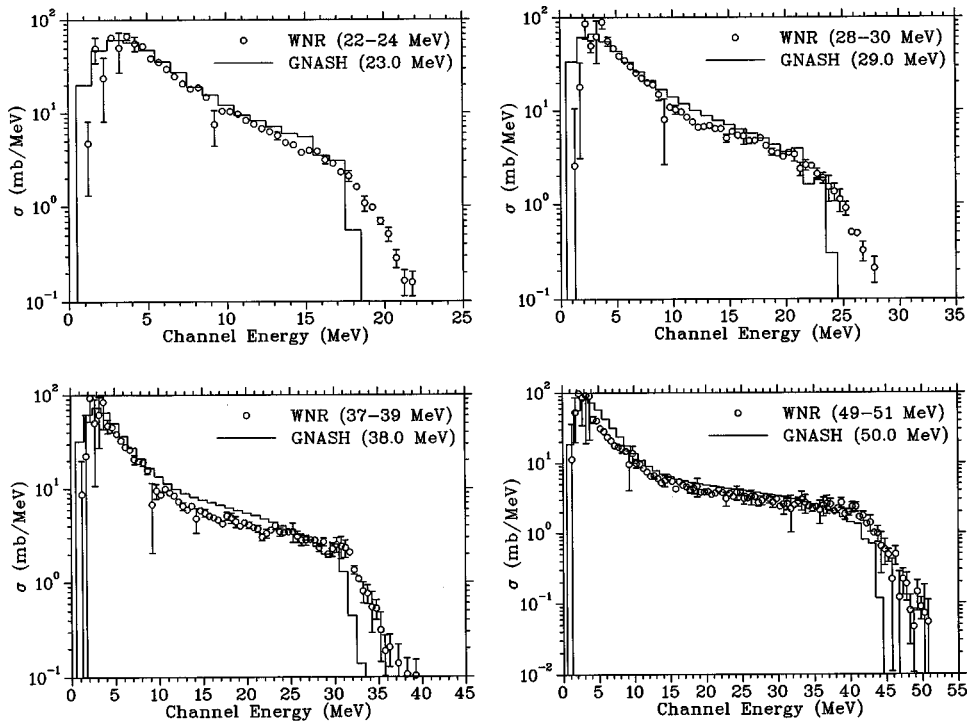

FIG. 8. Angle-integrated proton emission spectra for neutron energies of 22–24, 28–30, 37–39, and 49–51 MeV. The solid line depicts the results of GNASH calculations performed at the midpoint of the respective neutron energy bin.
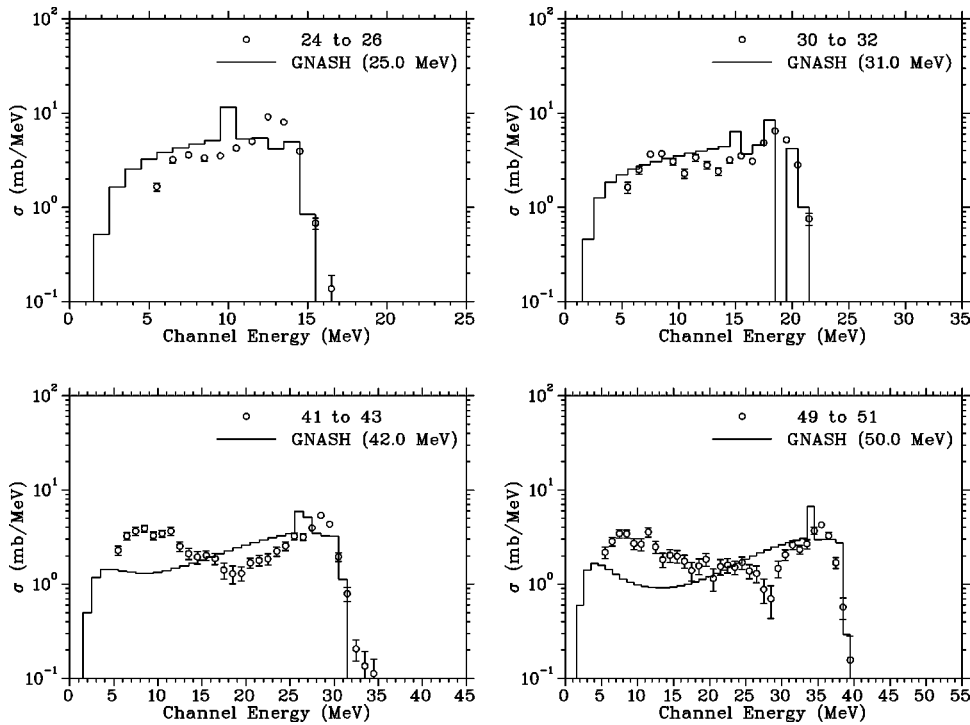
FIG. 9. Angle-integrated deuteron-emission spectra for neutron energies of 24–26, 30–32, 41–43, and 49–51 MeV. The solid line depicts the results of GNASH calculations performed at the midpoint of the respective neutron energy bin.

Finally, the angle-integrated spectra were integrated over emission energy to obtain the total production cross section for each charged-particle type. The results for alpha-particle production are given in Fig. 14 over the entire neutron energy range and in Fig. 15 up to 20 MeV, the range of most evaluated data sets and of most previous measurements. Statistical errors folded in with the uncertainty associated with fitting the angular distributions are shown. Systematic errors, mainly due to uncertainties in the ^{235}U fission foil thickness used to monitor the neutron flux and in the thickness of the (thin) silicon sample, add an additional $\sim 8\%$ normalization error to the data.

Compared with other alpha-particle production cross sections, our data show good agreement. Previously, these reactions have been studied near threshold with neutrons incident on silicon surface-barrier detectors. In this region, we choose the data of Birk *et al.* [35] as a representative data set. Near 14 MeV, the only available data are from the helium accu-
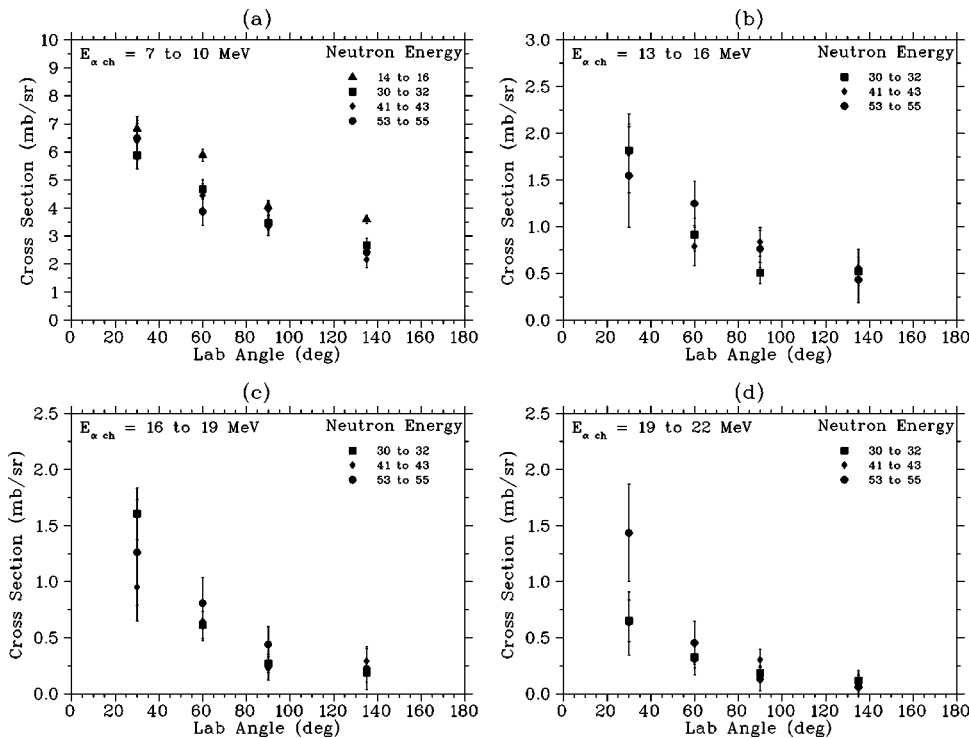

FIG. 10. Angular distributions of alpha-particles for (a) $E_\alpha = 7-10$ MeV, (b) $E_\alpha = 13-16$ MeV, (c) $E_\alpha = 16-19$ MeV, and (d) $E_\alpha = 19-22$ MeV for several incident neutron energy ranges.
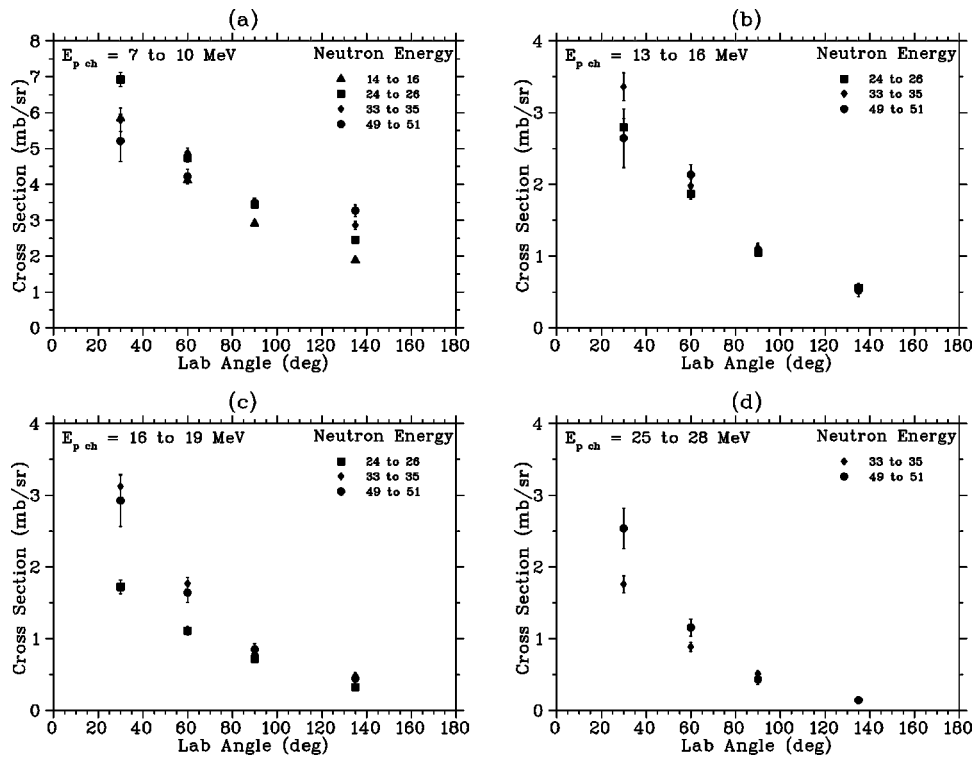
FIG. 11. Angular distributions of protons for (a) $E_p = 7$–10 MeV, (b) $E_p = 13$–16 MeV, (c) $E_p = 16$–19 MeV, and (d) $E_p = 25$–28 MeV for several incident neutron energy ranges. (Note that the neutron energies differ from those in Fig. 10.)

mulation measurements of Kneff *et al.* [36]

Figure 16 gives the total proton-production cross section results over the entire neutron energy range. The errors shown are the same as in Fig. 14. We estimate the normalization error of the proton data to be ∼10%, also due to uncertainties in the ^{235}U fission foil thickness, the thickness of the thick silicon sample, and the integration over angle. Because of the reaction kinematics, the spectra for low-energy protons have different threshold in channel energy depending on the angle at which the protons were detected. We have tried to compensate for this by assuming that the very-low-energy parts, below 3 MeV, of the spectra at 90° and 135° are the same as that observed at 60°, where the background was significantly less than at 30° in the proportional counter data. The resulting, ''corrected'' spectra are also given in Fig. 16. The crossing of the uncorrected and
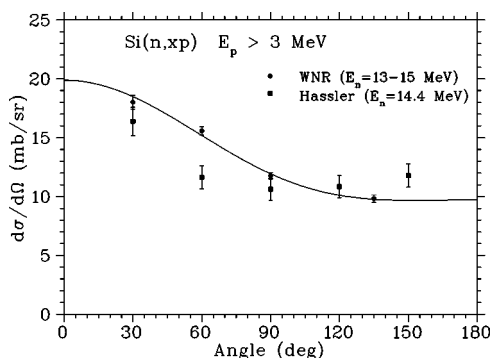

FIG. 12. Proton angular distributions at $E_n = 14$ MeV compared with Ref. [34]. Only protons above 3 MeV are integrated in this comparison. The line drawn through the present data represents a second-order Legendre polynomial fit.

corrected values above 30 MeV reflects the fact that the backgrounds for the low-energy part of the spectra were high at these higher neutron energies and therefore the statistical uncertainties in this part of the spectrum are large.

Proton-production results of the present experiment are compared in the region up to 20 MeV in Fig. 17 with illustrative results [37–39] of the many activation measurements (summarized in Ref. [40]), of a photographic plate method [41] and of reactions in a silicon detector [42]. Near 14 MeV the present results agree well with data in the literature. The effective threshold for the ^{28}Si(n,np) reaction is about 13 MeV (Q value is 11.98 MeV) so that the activation measurement of the ^{28}Si$(n,p)^{28}$Al reaction therefore measures the total proton production on this dominant isotope up to this energy. The decrease in the activation results [37] from 13 to 15 MeV indicates the opening of the (n,np) channel. The photographic plate [41] technique did measure all protons produced but only at one laboratory angle of 120°. The angle-integrated cross section was derived assuming isotropy, which is shown in Fig. 11 not to be a valid assumption. Because the angular distribution is somewhat forward peaked, the values of Ref. [41] can be expected to be somewhat lower than those of the present work.

Comparison of literature values with the present data below 9 MeV shows some similarities but also some disagreements. The high-resolution data of Refs. [38,39,42] have been averaged in 0.5 MeV bins in Fig. 17. Except for normalization factors, the shapes of the excitation functions are very similar. The unpublished data of Bass *et al.* [38] have a reported uncertainty of 10–15 %, whereas the overall normalization uncertainties are given to be 50% for the data of Marion *et al.* [39] and 30% for the data of Mainsbridge *et al.* [42]. The present data are lower on the order of 30% in this
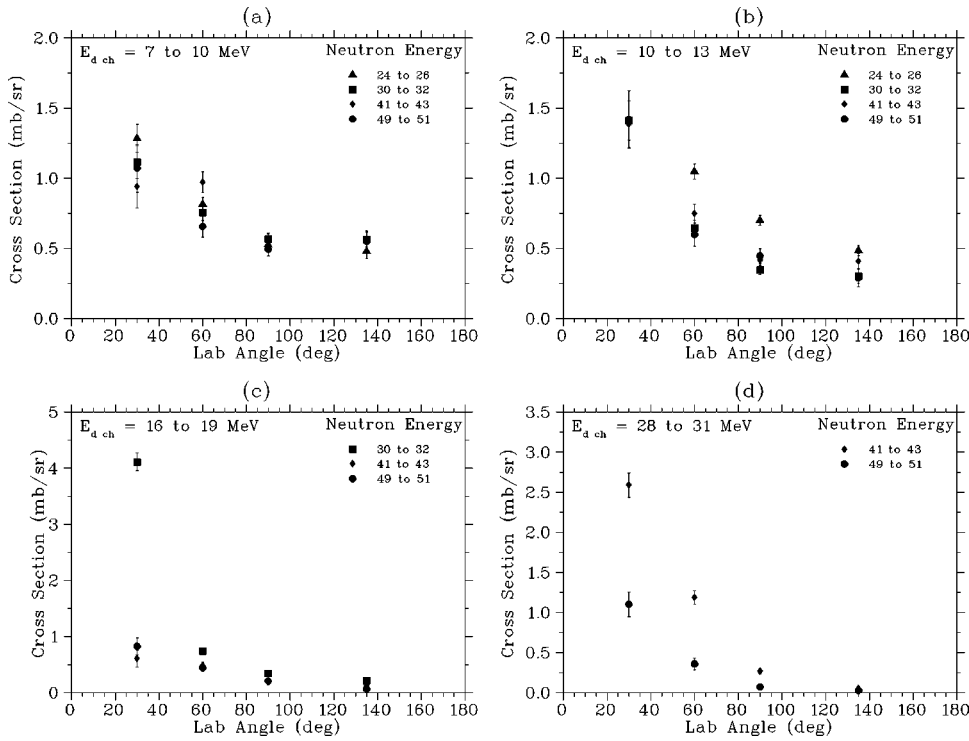
FIG. 13. Angular distributions of deuterons for (a) $E_d = 7-10$ MeV, (b) $E_d = 10-13$ MeV, (c) $E_d = 16-19$ MeV, and (d) $E_d = 28-31$ MeV for several incident neutron energy ranges. (Note that the neutron energies differ from those in Figs. 10 and 11.)

energy range (see Fig. 17). Other than our results, there are no data that cover the range from threshold to 14 MeV.

We have attempted unsuccessfully to resolve the discrepancy below 9 MeV in the proton-production cross sections. The fact that our data agree with activation data near 14 MeV gives us confidence in the overall normalization. Agreement of helium-production data (see Fig. 15) also adds confidence. Further activation measurements of the $^{28}Si(n,p)^{28}Al$ reaction could help clarify this discrepancy. Such measurements with broad neutron energy resolution in the region below 9 MeV could greatly reduce the uncertainties in the overall normalizations of previous activation data. Furthermore, if these measurements could extend into the 9–14 MeV range, the activation data could be compared with the trend of our proton-production cross sections.

At higher energies, proton production from silicon has also been investigated by Bharuth-Ram *et al.* [43] at 21.5

MeV and, slightly above the energy range of the present experiment, by Lambert *et al.* [44] (62.7 MeV) and Ullmann *et al.* [45] (59.1 MeV). All of these works report only partial cross sections either in the angular range or in proton energies detected due to the detection threshold. Their data are therefore not easily compared with ours. Qualitative agreement is generally seen, however, when our data are compared with these previous studies.

Deuteron total production cross sections for deuterons with energies above the detector threshold of about 5 MeV are given in Fig. 18. The uncertainties are similar to those for proton emission except for the increased uncertainty in integrating the more strongly forward-peaked angular distribu-
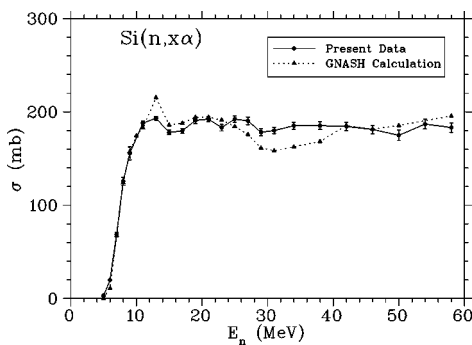

FIG. 14. Excitation function for alpha-particle production. The error bars represent statistical uncertainties. An additional normalization error is estimated to be $\sim 8\%$. Results of the GNASH calculation are indicated by the dotted line.
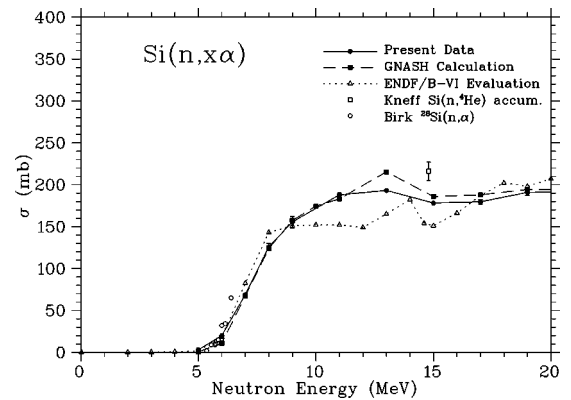

FIG. 15. Excitation function for alpha-particle production for neutron energies up to 20 MeV. The data points from the present experiment are the same as in Fig. 14. Experimental results of Birk *et al.* [35] (open circles), in which alpha particles were detected, and Kneff *et al.* [36], where the accumulated helium was measured, are shown. Results of the GNASH calculation are indicated by the dashed line and the ENDF/B-VI evaluation [40] by the dotted line.
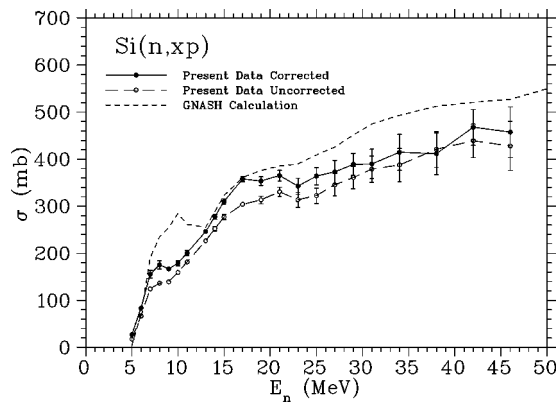
FIG. 16. Excitation function for proton production. The open circles represent the uncorrected cross section subject to the detection threshold of ~1.5 MeV in the laboratory. The solid circles are the threshold-corrected data based on the 60° detector results as described in the text. For both the uncorrected and corrected data, the error bars represent statistical errors; an additional normalization error is estimated to be ~10%. The dotted line is the GNASH calculation for all emission energies.

FIG. 18. Excitation function for deuteron production. The dashed line represents the uncompensated cross section subject to the detection threshold of ~5 MeV. The solid line indicates the threshold-corrected data based on the GNASH results while the dotted line is the GNASH calculation for all emission energies. The error bars represent statistical uncertainties. An additional normalization error is estimated to be ~15%.

tions. Many previous studies of deuteron production on silicon have concentrated only on population of a few low-lying residual states by direct reactions and are therefore not comparable to the present, total deuteron emission. The paper by Lambert *et al.* [44] presented some summary information on deuteron emission, but lack of space prohibited a more comprehensive description of their emission spectra in that pub-

lication. However, these authors noted the close similarity of their silicon and aluminum data, and the Al(n,xd) emission spectra reported in Ref. [46] bear a close similarity to our results shown in Fig. 9.

For applications, it is important to compare the present results with ENDF/B-VI evaluations [40] where the evaluated data have also been binned to smooth out the fluctuations below 9 MeV. For alpha-particle production (see Fig. 15), the present results vary more smoothly in energy than those of ENDF/B-VI but differ by no more than about 20% in the region above 8 MeV. For proton production (see Fig. 17), the agreement is good near 14 MeV, but the present results are less than ENDF/B-VI by up to 30% between 8 and 12 MeV and up to 20% in the 15–20 MeV range. The ENDF/B-VI evaluation for silicon does not extend to higher energies.

B. GNASH calculational results

Figures 7–9 show that, in general, the GNASH model calculations describe the measured spectra well. For protons and alphas, the calculations account for the shape and magnitude of the evaporation data at lower emission energies and the preequilibrium data at higher energies. For deuteron emission, the pickup model accounts for the general features of the high-energy deuteron emission, though some of the details of the measurements are not well reproduced; additionally, at higher incident energies the calculations underpredict the magnitude of deuteron compound-nucleus emission.

The present measurements of proton and alpha-particle emission extend to lower emission energies compared to most previous measurements. This allows the theoretical predictions of particle emission below the Coulomb barrier to be tested. Figures 7 and 8 show that the theoretical predictions are in generally good agreement with the data for low emission energies. The exception is alpha-particle emission at
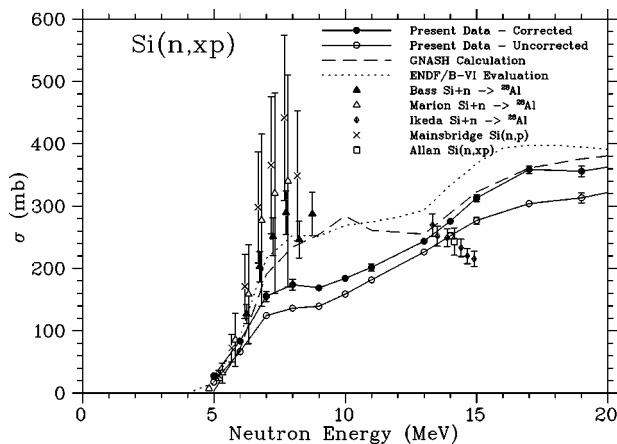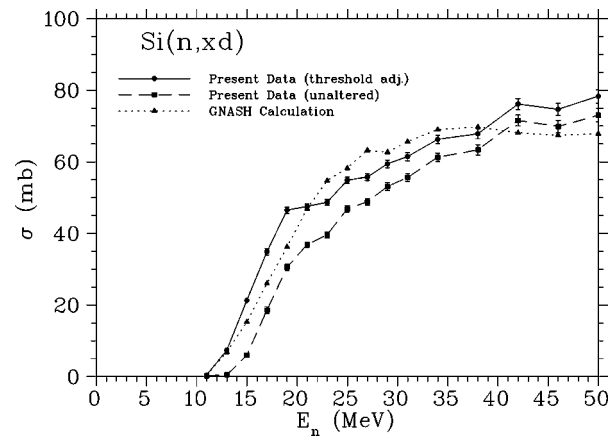

FIG. 17. Excitation function for proton production for neutron energies up to 20 MeV. The data points from the present experiment are the same as in Fig. 16. The dashed line indicates the results of the GNASH calculation while the dotted line represents the ENDF/B-VI evaluation [40]. Experimental results of Allan [41] are from detection of the protons, while those of Mainsbridge [*et al.* [42] are from interactions in a silicon detector. Activation measurements on ^{28}Si of Ikeda *et al.* [37], Bass *et al.* [38], and Marion *et al.* [39] are corrected to represent proton production through (n,p) reactions on the mixture of isotopes in natural silicon; the ^{28}Si$(n,p)^{28}$Al reaction accounts for nearly all of the proton production below 13 MeV. Absolute normalization uncertainties for data of Mainsbridge *et al.* and of Marion *et al.* are included in the data points; the relative uncertainties are much less.

about 2 MeV alpha-particle energy, for incident neutrons with energies below 26 MeV (upper panels of Fig. 7)—the calculated peak here is due to an apparent theoretical over-prediction of the ^{28}Si$(n,n'\alpha)$ channel.

Comparisons of calculated and measured total charged-particle production (integrated over all emission energies and angles) are shown in Figs. 14–18. Some general observations are given below, while detailed discussions on the impact of isospin conservation on these production cross sections is given in the next subsection.

The agreement between the calculated and measured alpha production in Fig. 14 is excellent. The calculation depends sensitively on the level densities used. While the level densities for the main competition processes (^{28}Si from neutron emission and ^{28}Al from proton emission) are known from other analyses, the level density for ^{25}Mg after alpha-particle emission was chosen so as to reproduce the experimental data in Fig. 14 below 10 MeV, and a level density was obtained that was consistent with neutron resonance measurements; see Sec. III B. It is therefore satisfying that the calculated alpha-particle production is in good agreement with measurements also at energies above 10 MeV, where multiparticle emission processes contribute to the inclusive alpha-production cross section.

Figures 16–18 show that the overall features of the measured proton and deuteron production cross sections are reproduced by the calculations, generally to better than 20%. However, the calculated proton production cross section in the 8–12 MeV range largely exceeds the present measurements: at 10 MeV incident energy, the discrepancy between theory and experiment amounts to approximately 30%. This large discrepancy is difficult to understand since the level densities and optical model transmission coefficients are known fairly well here, though isospin conservation would result in a smaller proton emission cross section as described in more detail below.

C. Isospin considerations

The GNASH calculations described above did not include the possibility of isospin conservation; indeed, few Hauser-Feshbach analyses of neutron-induced emission have included isospin effects. To address this question, we have made use of the work of Grimes [47] to assess the magnitude of this effect on charged-particle production. Adding isospin as a quantum number causes the addition of a Clebsch-Gordon coefficient to the decay width, reflecting the probability that the compound nucleus and ejectile isospin combine to yield the isospin of the final state. Since the alpha particle has isospin zero, it couples uniquely to a single value of isospin in the final nucleus. Both the proton and neutron have isospin 1/2; depending on whether the compound nucleus is neutron or proton rich, the proton or neutron, respectively, will couple to a unique isospin, but the other ejectile can reach two values of isospin in the final nucleus. One of these values corresponds to the population of levels with a much lower level density, so the introduction of isospin reduces the decay probability for ejectiles which couple to two different isospin values. We estimate about a factor of
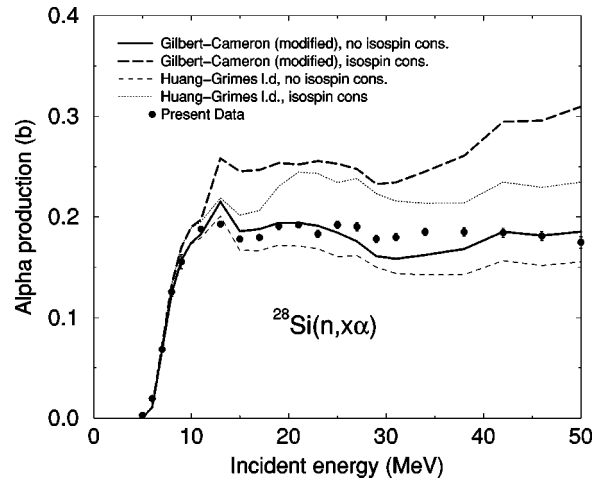

FIG. 19. Influence of isospin conservation on alpha production, for two different level density options in the calculations. If isospin mixing occurs at a level of approximately 50%, the results using the Huang-Grimes level densities (i.e., an average of the thin dashed and dotted lines) would agree reasonably well with the experimental data.

7 difference between the neighboring isospin $T_<$ and $T_>$ level densities, and therefore we ignore contributions from the smaller decay channels for simplicity. The extreme case is for a $T=0$ compound nucleus [e.g., produced in our example of reactions on silicon after an (n,n') reaction] for which the coupling for both protons and neutrons is 1/2, greatly enhancing the probability for alpha decay compared to a calculation without isospin. The enhancement or reduction factors for the entire spectrum at a given bombarding energy are averages over the factors for each decaying compound nucleus. A net enhancement of about 30% for alphas is found, while proton and neutrons are reduced by about 9% and 2%, respectively. Similar effects are seen in the minor decay channels, with an enhancement for deuterons and reductions for tritons and ^{3}He particles.

Figure 19 shows the effect of isospin conservation on calculated alpha production for two different level density approaches: (1) our default level density calculations described in Sec. III (i.e., ^{28}Si and ^{28}Al based on level density experimental data, ^{25}Mg densities chosen to optimize agreement with the alpha-production measurements reported here, and other nuclei level densities taken from Cook systematics) and (2) Huang-Grimes systematics [23] for the $A=20$–40 mass region. In both cases, the assumption of 100% isospin conservation results in a significant increase in alpha production for incident energies above approximately 10 MeV.

When no isospin conservation was included, our default calculations shown by the solid line account for alpha-production measurements well—as they should since the ^{25}Mg level density was chosen to result in a good agreement for low incident energies. The calculations using the Huang-Grimes level density systematics with no isospin conservation underpredicted the experimental data, primarily because of a lower level density for ^{25}Mg. With 100% isospin conservation the calculations using the Huang-Grimes level density then somewhat overpredict the data. However, other

studies of isospin conservation in Hauser-Feshbach reactions have pointed to an isospin conservation level of about 50% [48] and a 50% mixing; i.e., a curve, given by the average of the thin dashed and dotted lines in Fig. 19, would result in a reasonable agreement with the data.

Given that the systematic behavior of the Huang-Grimes level densities is based on a wide variety of experimental information, the densities are thought to be fairly reliable for nuclides such as ^{25}Mg, which influence alpha production. The fact that calculations without isospin conservation underpredict the alpha production data, but result in reasonable agreement when 50% isospin conservation is assumed, provides support for the importance of isospin conservation in neutron-induced reactions where the target isospin is small. We admit, though, that this argument would be stronger if the ^{25}Mg level density were better known from direct measurements, rather than from systematical behaviors as embodied in Huang-Grimes systematics.

V. CONCLUSIONS

New measurements of proton, deuteron, and alpha-particle production have been made for neutrons on natural silicon from threshold to 60 MeV with a spallation neutron source. Emission spectra, angular distributions, and production cross sections are reported here and compared with literature data where available, with evaluated nuclear data files up to 20 MeV, and nuclear reaction model calculations. The reaction models are able to reproduce the proton and alpha-particle emission data quite well and to account for some of the features of deuteron production. Inclusion of isospin in the reaction models is shown to increase the calculated production cross section for alpha particles by about 30% and to decrease the proton-production cross section by about 9%. These changes then require changes in the input parameters such as the nuclear level densities to bring the calculated cross sections back into agreement with experiment.

[1] J. F. Ziegler and W. A. Lanford, Science **206**, 776 (1979).

[2] C. A. Gossett, B. W. Hughlock, M. Katoozi, G. S. LaRue, and S. A. Wender, IEEE Trans. Nucl. Sci. **NS-40**, 1845 (1993).

[3] E. Normand, J. L. Wert, P. P. Majewski, D. L. Oberg, W. G. Bartholet, S. K. Davis, M. Shoga, S. A. Wender, and A. Gavron, in *Proceedings of the IEEE Radiation Effects Data Workshop* (IEEE Nuclear and Plasma Sciences Society, The Institute of Electrical and Electronic Engineers, Inc., 1995), p. 33.

[4] E. Normand and T. J. Baker, IEEE Trans. Nucl. Sci. **NS-40**, 1484 (1993).

[5] W. Hauser and H. Feshbach, Phys. Rev. **87**, 366 (1952).

[6] H. Vonach, in ''Proceedings of the IAEA Advisory Group Meeting on Basic and Applied Problems of Nuclear Level Densities,'' Brookhaven National Laboratory, Upton, NY, 1983, Brookhaven National Laboratory Report No. BNL-NSC-51694, p. 247.

[7] T. Ericson, Phys. Rev. Lett. **5**, 430 (1960).

[8] T. Ericson, Ann. Phys. (N.Y.) **23**, 340 (1963).

[9] W. P. Abfalterer, R. W. Finlay, S. M. Grimes, and V. Mishra, Phys. Rev. C **47**, 1033 (1993).

[10] S. M. Grimes, S. D. Bloom, H. K. Vonach, and R. F. Hausman, Phys. Rev. C **27**, 2893 (1983).

[11] F. B. Bateman, S. M. Grimes, N. Boukharouba, V. Mishra, C. E. Brient, R. S. Pedroni, T. N. Massey, and R. C. Haight, Phys. Rev. C **55**, 133 (1997).

[12] P. W. Lisowski, C. D. Bowman, G. J. Russell, and S. A. Wender, Nucl. Sci. Eng. **106**, 208 (1990).

[13] S. M. Grimes, R. C. Haight, C. E. Brient, F. C. Goeckner, F. B. Bateman, M. B. Chadwick, T. M. Lee, S. M. Sterbenz, P. G. Young, O. A. Wasson, and H. Vonach, Nucl. Sci. Eng. **124**, 271 (1996).

[14] R. C. Haight, F. B. Bateman, S. M. Sterbenz, S. M. Grimes, O. A. Wasson, P. Maier-Komor, and H. Vonach, Fusion Eng. Des. **37**, 73 (1997).

[15] D. Horn, G. C. Ball, A. Galindo-Uribarri, E. Hagberg, R. B. Walker, R. Laforest, and J. Pouliot, Nucl. Instrum. Methods Phys. Res. A **320**, 273 (1992).

[16] N. R. Yoder, technical report, Indiana University, Bloomington, Indiana (unpublished).

[17] P. G. Young, E. D. Arthur, and M. B. Chadwick, in *Proceedings of the IAEA Workshop on Nuclear Reaction Data and Nuclear Reactors—Physics, Design, and Safety*, Trieste, Italy, 1996, edited by A. Gandini and G. Reffo (World Scientific Publishing, Singapore, 1998), pp. 227–404.

[18] C. Kalbach, Z. Phys. A **283**, 401 (1977).

[19] M. B. Chadwick, P. G. Young, D. C. George, and Y. Watanabe, Phys. Rev. C **50**, 996 (1994).

[20] A. Gilbert and A. G. W. Cameron, Can. J. Phys. **43**, 1446 (1965).

[21] *Handbook for Calculations of nuclear reaction data: Reference input parameter library* (International Atomic Energy Agency, Vienna, Austria, 1998), http://www-nds.iaea.or.at/ripl, No. IAEA-TECDOC-1034.

[22] J. L. Cook, H. Ferguson, and A. R. Musgrove, Aust. J. Phys. **20**, 477 (1967).

[23] P. Huang, S. M. Grimes, and T. N. Massey, Phys. Rev. C (submitted).

[24] G. M. Braga-Marcazzan and L. Milazzo-Colli, Energ. Nucl. (Italy) **15**, 186 (1968).

[25] J. Raynal, Technical Report No. CEA-N-2772, Commissariat à l'Energie Atomique (CEA), Saclay, France (unpublished), pp. 1–145.

[26] D. G. Madland, in *Proceedings of a Specialists Meeting on Preequilibrium Reactions*, Semmering, Austria, 1988, edited by B. Strohmaier [Organization for Economic Cooperation and Development (OECD) Nuclear Energy Agency, Paris, France, 1988], No. NEANDC-245, pp. 103–116.

[27] R. Alarcon and J. Rapaport, Nucl. Phys. **A458**, 502 (1986).

[28] F. D. Becchetti and G. W. Greenlees, in *Proceedings of the Conference on Polarization Phenomena in Nuclear Reactions*, edited by H. Barschall and W. Haeberli (University of Wisconsin Press, University of Wisconsin, 1971), p. 682.

[29] C. M. Perey and F. G. Perey, At. Data Nucl. Data Tables **17**, 1 (1976).

[30] L. McFadden and G. R. Satchler, Nucl. Phys. **84**, 177 (1966).

[31] L. Colli, G. M. Marcazzan, F. Merzari, P. G. Sona, and P. Tomas, Nuovo Cimento **20**, 928 (1961).

[32] D. Hilscher, H. H. A. Morgenstern, and J. A. Scheer, Z. Phys. **183**, 77 (1965).

[33] C. Kalbach, Phys. Rev. C **37**, 2350 (1988).

[34] F. L. Hassler and R. A. Peck, Phys. Rev. **125**, 1011 (1962).

[35] M. Birk, G. Goldring, and P. Hillman, Nucl. Instrum. Methods **21**, 197 (1963).

[36] D. W. Kneff, B. M. Oliver, H. Ferrar, and L. R. Greenwood, Nucl. Sci. Eng. **92**, 491 (1986).

[37] Y. Ikeda, C. Konno, K. Oishi, T. Nakamura, H. Miyade, K. Kawade, H. Yamamoto, and T. Katoh, Technical Report No. JAERI-1312, Japan Atomic Energy Research Institute, Tokai, Japan (unpublished).

[38] R. Bass, P. Haug, K. Kruger, and B. Staginnus, Report EANDC(E) 66''U,'' 1966, p. 64.

[39] J. B. Marion, R. M. Brugger, and R. A. Chapman, Phys. Rev. **101**, 247 (1956).

[40] D. M. Hetrick, D. C. Larson, N. M. Larson, L. C. Leal, and S. J. Epperson, Technical Report No. ORNL/TM-11825, Oak Ridge National Laboratory, Oak Ridge, TN (unpublished).

[41] D. L. Allan, Nucl. Phys. **24**, 274 (1961).

[42] B. Mainsbridge, T. W. Bonner, and T. A. Rabson, Nucl. Phys. **48**, 83 (1963).

[43] K. Bharuth-Ram, S. M. Perez, F. D. Brooks, S. A. R. Wynchank, and W. R. McMurray, Nucl. Phys. **A278**, 285 (1977).

[44] M. Lambert, S. Benck, I. Slypen, V. Corcalciuc, and J. P. Meulders, in *Proceedings of the International Conference on Nuclear Data for Science and Technology*, Trieste, Italy, 1997, edited by G. Reffo (Societa Italiana di Fisica, Bologna, Italy, 1997), pp. 1516–1518.

[45] J. L. Ullmann, F. P. Brady, D. H. Fitzgerald, G. A. Needham, J. L. Romero, and C. M. Castaneda, Nucl. Phys. **A386**, 179 (1982).

[46] S. Benck, I. Slypen, J. P. Meulders, V. Corcalciuc, M. B. Chadwick, P. G. Young, and A. J. Koning, Phys. Rev. C **58**, 1558 (1998).

[47] S. M. Grimes, Phys. Rev. C **46**, 1064 (1992).

[48] C. R. Lux, N. T. Porile, and S. M. Grimes, Phys. Rev. C **15**, 1308 (1977).